AGU PUBLICATIONS

JGR

Journal of Geophysical Research: Oceans

RESEARCH ARTICLE

10.1002/2015JC010886

Key Points:
- Coastal upwelling signal along the coast of Sumatra/Java
- Long-term sea level observations by Indonesian tidal stations
- Intraseasonal coastal upwelling signal linked to local SST

Supporting Information:
- Supporting Information S1

Correspondence to:
T. Horii,
horiit@jamstec.go.jp

Citation:
Horii, T., I. Ueki, F. Syamsudin, I. Sofian, and K. Ando (2016), Intraseasonal coastal upwelling signal along the southern coast of Java observed using Indonesian tidal station data, *J. Geophys. Res. Oceans*, *121*, 2690–2708, doi:10.1002/2015JC010886.

Received 30 MAR 2015
Accepted 18 MAR 2016
Accepted article online 22 MAR 2016
Published online 21 APR 2016

Intraseasonal coastal upwelling signal along the southern coast of Java observed using Indonesian tidal station data

Takanori Horii[1], Iwao Ueki[1], Fadli Syamsudin[2], Ibnu Sofian[3], and Kentaro Ando[1]

[1]Research and Development Center for Global Change, Strategic Research and Development Area, Japan Agency for Marine-Earth Science and Technology, Yokosuka, Japan, [2]Indonesian Agency for the Assessment and Application of Technology, Jakarta, Indonesia, [3]Geospatial Information Agency, Bogor, Indonesia

Abstract Sea level variations along the coasts of Sumatra and Java were investigated to determine the coastal upwelling signal that is linked to local sea surface temperature (SST) variability. We used Indonesian tidal station data together with satellite SST data and atmospheric reanalysis data. The sea level variations along the southern coast of Java have a significant coherence with remote wind, local wind, and local SST variations, with an intraseasonal time scale of 20–50 days. Assuming that a coastal upwelling signal would appear as a sea level drop (SLD), we focused on intraseasonal-scale SLD events in the data. Significant upwelling signals are frequently observed during both the boreal summer and winter. To evaluate the impact of the coastal upwelling on local SST, we examined statistical relationships between sea level and SST variations. The results demonstrated that events that occurred during April–August were associated with local SST cooling. The horizontal distribution of the SST cooling was analogous with annual mean SST, suggesting the importance of intraseasonal-scale coastal upwelling in forming the climatic conditions of the southeastern tropical Indian Ocean.

1. Introduction

The Indian Ocean warm pool is an area of active air-sea interaction induced by the high SST and the surrounding SST gradient (see *Schott et al.* [2009] for a review). Sumatra and Java in Indonesia are located in the warm pool, and form part of the eastern boundary of the tropical Indian Ocean (Figure 1). It has been reported that there are coastal upwelling phenomena along the southwestern coasts of the islands due to the prevailing southeasterly wind during the boreal summer monsoon [e.g., *Wyrtki*, 1962; *Bray et al.*, 1996; *Susanto et al.*, 2001]. The coastal upwelling system is robust enough for the signals to be detected using reconstructed ocean temperature data on a millenarian time scale [*Steinke et al.*, 2014]. Because coastal upwelling brings cool and nutrient-rich water to the ocean surface, it plays an important role in the ocean surface heat and biogeochemical balance in the area. In the annual mean SST, relatively cool water, determined by the 28°C isotherm, outcrops off the southern coast of Java (Figure 1a), which must be a result of coastal upwelling. The annual mean SST pattern implies that coastal upwelling can potentially have an impact on the formation of regional climate conditions in the area.

Coastal upwelling along the coasts of Sumatra and Java develops in June–September [e.g., *Susanto et al.*, 2001]. During the summer monsoon, a southeasterly monsoonal wind prevails along the coasts and surrounding offshore areas. Resultant Ekman transport and coastal upwelling replaces surface warm water with cool water from underneath [*Wyrtki*, 1962; *Bray et al.*, 1996; *Susanto et al.*, 2001]. Understanding equatorial and coastal Kelvin waves is also important because the coastal upwelling system can interact with the Kelvin wave propagation [*Murtugudde et al.*, 2000]. Previous studies have indicated that remotely and locally forced coastal Kelvin waves, and their propagation, can have marked impacts on the hydrographic conditions off the coasts of Sumatra and Java [*Yamagata et al.*, 1996; *Sprintall et al.*, 2003; *Syamsudin and Kaneko*, 2013].

Coastal upwelling along the coasts of Sumatra and Java has been studied not only as an annual signal in response to southeasterly wind in the boreal summer, but also as a signal closely related to the El Niño/Southern Oscillation (ENSO) [e.g., *Susanto et al.*, 2001; *Susanto and Marra*, 2005]. The upwelling also plays a key role in the independent ocean-atmosphere mode in the Indian Ocean, i.e., the so-called Indian Ocean

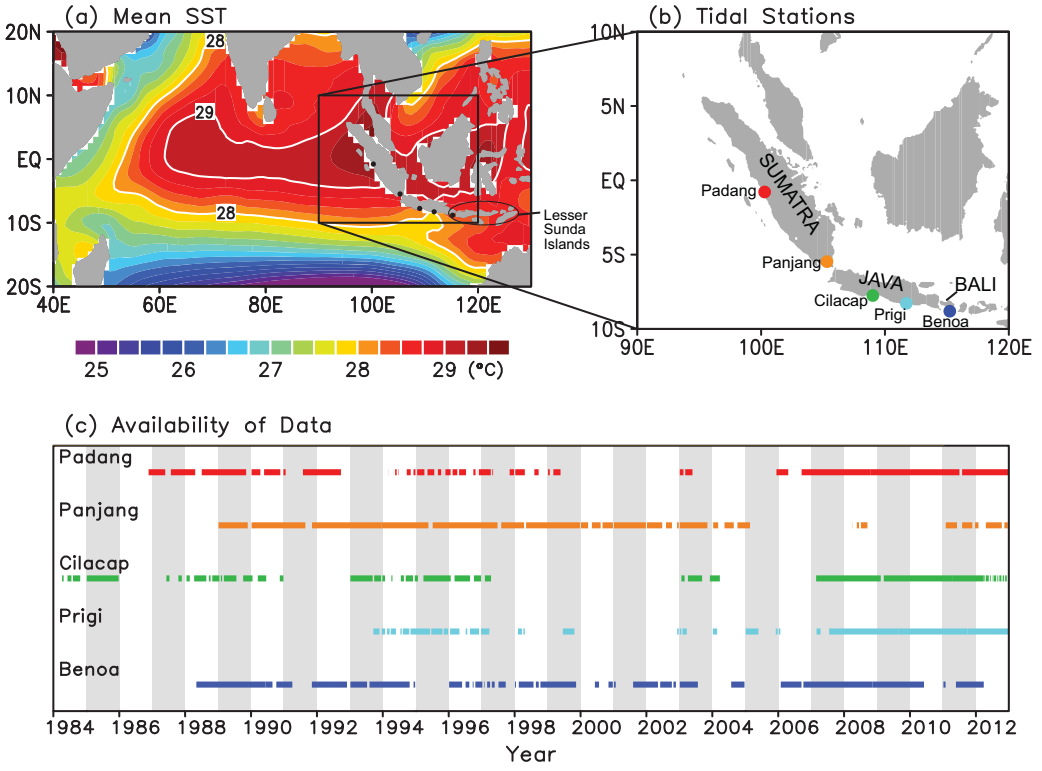

Figure 1. (a) Annual mean SST obtained from the National Oceanic and Atmospheric Administration Optimum Interpolation data set from 1982 to 2010 [*Reynolds et al.*, 2002]. The 28°C and 29°C contours are highlighted. (b) Locations of the Indonesian tidal stations used in this study. (c) Availability of tidal station data at Padang (red), Panjang (orange), Cilacap (green), Prigi (light blue), and Benoa (dark blue) for the period 1984–2012.

Dipole (IOD), which develops in the boreal summer and fall [e.g., *Saji et al.*, 1999; *Webster et al.*, 1999]. Using satellite-observed SST and sea level anomalies (SLA), *Susanto et al.* [2001] showed that the strength of the upwelling along the coasts of Sumatra and Java was closely linked to the ENSO. *Ningsih et al.* [2013] reported the same results, also using satellite-observed chlorophyll *a* data, with a focus on the upwelling signals along the coast of Bali and further east to the Lesser Sunda Islands. In the development of a positive IOD, the upwelling of cool subsurface water along the coasts, and its westward expansion, produce a large SST gradient in the central-eastern tropical Indian Ocean. The resultant atmospheric pressure gradient produces southeasterly wind anomalies along the coasts, and the wind anomalies strengthen the SST gradient through enhancement of the upwelling and cause Bjerknes feedback. This ocean-atmosphere feedback process was originally described by *Saji et al.* [1999] and *Webster et al.* [1999], and has been reproduced by numerical models [e.g., *Murtugudde et al.*, 2000; *Iizuka et al.*, 2000; *Vinayachandran et al.*, 2002; *Halkides and Lee*, 2009], and also identified by in situ observations [*Horii et al.*, 2009]. Thus, coastal upwelling along the Indonesian coast is considered to be an essential element of the ocean-atmosphere coupling system in the eastern Indian Ocean.

To understand coastal upwelling as a part of the ocean-atmosphere coupling system, we need to clarify the actual process in which the upwelling event is linked to local SST. Ocean thermal variation due to coastal upwelling can be seen approximately in thermocline fluctuation, and hence can be discerned from sea level variations [*Charney*, 1955; *Yoshida*, 1955; *Gill and Clarke*, 1974]. *Iskandar et al.* [2005] investigated sea level variations along the coasts of Sumatra and Java using Indonesian tidal station data, with a focus on the intraseasonal time scale. In their study, the sea level variations were well reproduced using the analytical model of *Gill and Clarke* [1974] forced by wind stress. They demonstrated that the intraseasonal sea level variations could be explained by both local and remote wind forcing, and the resultant propagation of coastal Kelvin waves. They also found that the sea level variations were characterized by a pronounced intraseasonal spectral peak, with a time scale of 20–40 (60–90) days in the boreal summer (winter). An adjustment of the coastal upwelling system could be accomplished within the time scale of Ekman

transport, which is in the order of a few days or weeks [e.g., *Charney*, 1955; *Yoshida*, 1955]. On the basis of the short time scale of the adjustment and the results in *Iskandar et al*. [2005], it was suggested that coastal upwelling signals and their possible linkage to SST might also be observed in the intraseasonal period.

To date, very few observational studies have reported intraseasonal coastal upwelling signals and their possible link to local SST along the coasts of Sumatra and Java. The previous studies [*Susanto et al*., 2001; *Susanto and Marra*, 2005; *Ningsih et al*., 2013] used satellite-based observations to observe the signal, and mainly studied seasonal to interannual signals. Further study is required to understand the ocean-atmosphere interactions associated with intraseasonal coastal upwelling signals. To consider these intraseasonal signals, we examined sea level variations along the southern coast of Java using Indonesian tidal station data. We also observed atmospheric and oceanic variations associated with the coastal upwelling signals using atmospheric reanalysis data and high-resolution satellite-measured SST data. Our aim was to understand the intraseasonal coastal upwelling system that produces local SST variations, which can then have an impact on regional climate.

The remainder of this paper is organized as follows. Section 2 presents the data sets and data processing procedures. Section 3 examines the time scale of the coastal upwelling signals, and their statistical relationship with atmospheric forcing and local SST. Section 4 focuses on the signals observed in the boreal summer, and investigates the atmospheric and oceanic variations related to significant coastal upwelling events. The results and implications are discussed in section 5, followed by a summary and conclusions in section 6.

2. Data and Processing

2.1. Sea Level Data

We used hourly sea level data from tide gauges along the southwestern-southern coasts of Sumatra, Java, and Bali (Figure 1). These data were originally collected by the Indonesian Geospatial Information Agency (BIG: Badan Informasi Geospasial in Indonesian). The sea level data at Padang, Cilacap, Prigi, and Benoa are registered as Research Quality Data at the University of Hawaii Sea Level Center (UHSLC) (http://uhslc.soest.hawaii.edu). The quality control was conducted by comparing hourly original data with predicted tides obtained by a harmonic analysis [*Foreman*, 1977]: gaps of less than 25 h were smoothly interpolated using predicted tides. Timing errors were corrected by shifting the data. Reference level shifts were corrected only if local information was available, and data with unresolved datum shifts were removed. For more information, see http://ilikai.soest.hawaii.edu/rqds/README.

We also used hourly sea level observations along the southern coast of Sumatra (Panjang; Figure 1b) collected by BIG. We also used data from intermittent sea level observations at Padang (1993–2003) and Prigi (1993–2005), which were not registered at UHSLC, but were archived in BIG.

For all of the data obtained from UHSCL and BIG, we again performed quality control with visual checks of the original hourly data, predicted tides, and the differences (residuals) year by year. In our quality control, the predicted tides and the residuals were computed using a harmonic analysis [*Foreman*, 1977; *Pawlowicz et al*., 2002]. We removed any data with suspicious jumps, datum shifts, and time shifts. Time series of less than 1 month were also discarded.

2.2. Processing

We calculated a daily sea level anomaly time series from the original using the following procedure. First, barometric effects were corrected by subtracting the sea level pressure data obtained from the European Centre for Medium-Range Weather Forecasts (ECMWF) reanalysis data. The original six-hourly pressure data were interpolated into hourly values using the Akima spline method [*Akima*, 1970]. We found that the variances from atmospheric forcing were less than 4% in each observation station. Second, sea level anomalies were calculated from the temporal mean of each time series, after separating out data with a long data gap (i.e., more than 1 year). This procedure was applied to remove any datum shifts that remained in the data, although it naturally ruled out any decadal variability in the time series. Third, short gaps of less than 5 days (120 h) were interpolated by applying a harmonic analysis. Here we calculated the tidal constituents using the T_Tide harmonic analysis package [*Pawlowicz et al*., 2002] based on the 1 year data around the period, and smoothly interpolated the gaps using the predicted tides and linear trend for the relevant period.

Table 1. Correlation Coefficients Among the Sea Level Data From the Stations[a]

	Panjang	Cilacap	Prigi	Benoa
Padang	**0.756** (+1)	0.642 (+3)	0.520 (+4)	0.441 (+6)
Panjang		**0.764** (+1)	0.542 (+3)	0.640 (+4)
Cilacap			**0.820** (+1)	**0.765** (+2)
Prigi				**0.709** (+1)

[a]To remove the effect of a datum shift, results were obtained from two time series of the temporal changes in the sea level ($\partial/\partial t$) calculated by central differences. The maximum correlation is shown with the lag (days) (e.g., the sea level at Padang leads that at Panjang by 1 day). Correlations > 0.7 are shown in bold characters. In case of the correlation coefficient of 0.7, the confidence interval was 0.50–0.84.

Finally, we applied a 48 h tide killer filter [*Hanawa and Mitsudera*, 1985] to remove the high-frequency variability that was mainly associated with semidiurnal and diurnal tides, and simply averaged the hourly data to daily data.

The locations of the five tidal stations and the time period over which data were collected are shown in Figure 1. Although there were a number of gaps, these tidal data provide an unprecedented observational time series from 1984 to 2012 (29 years) in the eastern boundary area of the tropical Indian Ocean. *Bray et al*. [1996] and *Iskandar et al*. [2005] also used the same data in climate studies, but analyzed the data for a short period of less than 3 years.

To check reliability of the data, we calculated the correlation coefficients for the relationships between each pair of the five stations (Table 1). Each correlation was statistically significant at the 99% level and the correlation coefficient of two adjacent stations was high (>0.7), which suggested that the observational data were reliable. The significant correlations and respective time lags (Table 1) suggested that the signals were propagated along the coasts by coastal Kelvin waves, as discussed by *Iskandar et al*. [2014].

2.3. Other Data Sources

We used other data sources to study large-scale oceanic and atmospheric variations related to coastal sea level variations. Satellite-observed sea level anomalies (SLA) were obtained from the SSALTO/DUACS multimission altimeter products from Archiving, Validation and Interpretation of Satellite Oceanographic data (AVISO) (http://www.aviso.altimetry.fr). The along-track SLA data were measured by the TOPEX/POSEIDON, JASON-1, and JASON-2 satellites. The repeat cycle of the satellite observations is approximately 10 days. Although the data from AVISO also provide sea level time series longer than 20 years, they do not resolve the intraseasonal signal well, as shown in section 3. Therefore, we used them mainly to validate the in situ sea level observation data (see Appendix A1). We also used their gridded SLA products: Mapped SLA (MSLA). We used the 2014 version data, in which the reference period is based on a 20 year period (1993–2012).

To observe SST in the tropical Indian Ocean, including the area off the coasts of Sumatra and Java, we used SST data obtained from the Tropical Rainfall Measuring Mission (TRMM) Microwave Imager (TMI) [*Wentz*, 1997]. We applied a spatial Gaussian filter with the horizontal *e*-folding scale of 0.5° × 0.5° to the original 3 day average product (0.25° × 0.25°), interpolated missing values spatially, and regridded them onto a 1° × 1° horizontal resolution. The TMI SST was available from December 1997 onward. We repeated the entire analysis using the National Oceanic and Atmospheric Administration (NOAA) daily optimum interpolation (OI) SST data set on a 0.25° × 0.25° grid [*Reynolds et al*., 2007] and obtained almost the same results. We also used the NOAA weekly OI SST data set on a 1° × 1° grid [*Reynolds et al*., 2002] to observe climatological mean SST (Figure 1a). Daily surface wind fields were obtained from the National Centers for Environmental Prediction (NCEP)/National Center for Atmospheric Research (NCAR) reanalysis data set [*Kalnay et al*., 1996]. To observe oceanic and atmospheric signals and their evolution with Hovmoller diagrams, we calculated the data along the equator and Indonesian coasts (Sumatra, Java, and Bali) using the spatial Gaussian filter with the horizontal *e*-folding scale of 0.5° × 0.5°.

To evaluate the air-sea heat exchange, the daily TropFlux data set [*Praveen Kumar et al*., 2012] for the period of 2007–2012 was used. In the TropFlux data set, turbulent heat fluxes were estimated from a combination of satellite observation data and reanalysis data. The shortwave radiation was based on the International Satellite Cloud Climatology (ISCCP) data set [*Zhang et al*., 2004] by 2009, and was extended by an estimate using outgoing longwave radiation (OLR). The longwave radiation was estimated using an empirical formula [*Clark et al*., 1974]. The data set was available on a 1° × 1° grid.

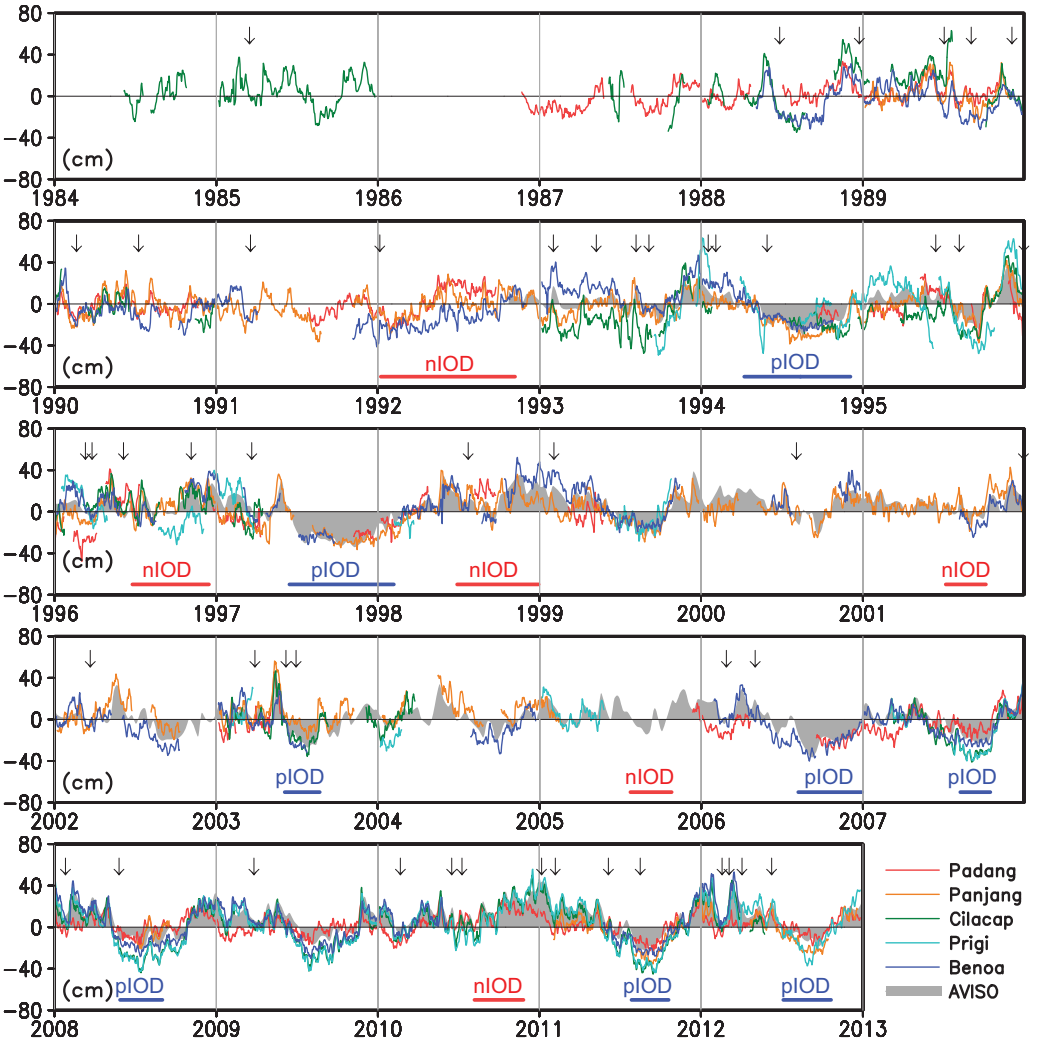

Figure 2. Time series of sea level anomalies (cm) obtained from five tidal stations along the southern coasts of Sumatra, Java, and Bali. The colors of the time series are as in Figure 1. The gray shades indicate sea level anomalies obtained from the AVISO along-track product near the Cilacap station (8°S, 109°E). The along-track SLA data with the original 10 day interval were interpolated smoothly for display, using the Akima spline method. The blue and red bar denote the period of positive IOD (pIOD) and negative IOD (nIOD) events, respectively, defined by 3 month running-mean dipole mode index [*Saji et al.*, 1999] and the one standard deviation. Sea level drop (SLD) events sampled on the basis of 2.0 standard deviations are shown with arrows (see section 4.1).

3. Intraseasonal Sea Level Variations

The observed sea level data displayed intraseasonal, seasonal, and interannual variations (Figure 2). In general, the sea level was lower during the boreal summer monsoon (June–September) when southeast monsoonal winds prevailed along the coasts of Sumatra and Java. The sea level amplitude was usually larger at Java and Bali than at Sumatra. Intraseasonal fluctuations were observed both during the winter monsoon (December–March) and the summer monsoon, as shown in *Iskandar et al.* [2005]. These variations occurred almost every year, although the data in the 1980s were sparse. There were pronounced seasonal sea level depressions that were particularly large and prolonged in 1994, 1997, and 2006, when the large positive IOD occurred. In contrast, the seasonal depression was not clear in 1996, 1998, and 2010, probably because a large negative IOD occurred around August–October in these years.

Satellite-observed along-track SLA began in late 1992 and also revealed seasonal and interannual variations off the southern coast of Java (Figure 2). Note that intraseasonal variability, especially on a submonthly time scale, was not well captured by the satellite observations because of the observation cycle (every 10 days). The satellite observations and in situ sea level data were consistent in recent years, especially after 2006.

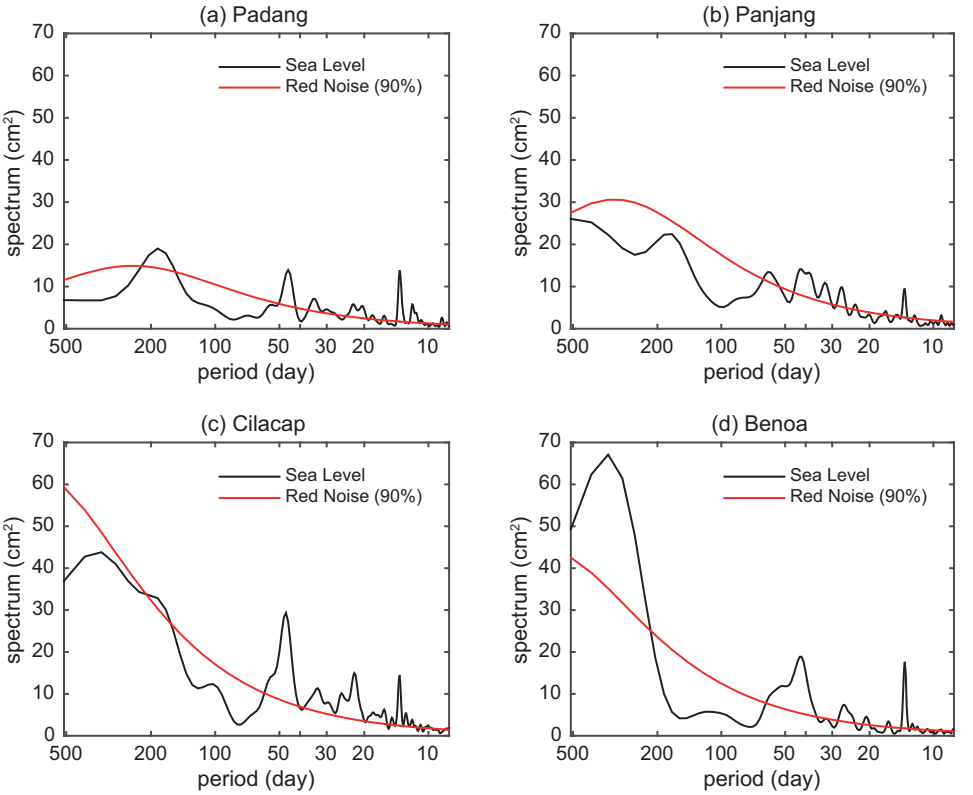

Figure 3. Variance-preserving spectra of the sea level at four tidal stations: (a) Padang, (b) Panjang, (c) Cilacap, and (d) Benoa. A Hanning filter was applied 10 times to smooth the spectra. The red line denotes the 90% confidence limits of the theoretical red noise background (the degree of freedom was estimated to be 16).

This suggests that the sea level data have become more reliable, and also implies that datum shifts remain in the data, particularly in 1993. In this study, we mainly used sea level data for the period after 2006. Data for the period before 2006 were used to construct statistics regarding significant sea level drops (section 4). Here to avoid effects from datum shift, we discussed the temporal changes only when the time series contained no significant gaps.

To confirm the dominant periods of sea level variability, we computed the power spectra (Figure 3). We selected 2048 day time series for the stations at Padang and Panjang. For Cilacap and Benoa stations, we used 1859 day and 1588 day time series instead, with zero padding, respectively. Data for Prigi are not shown here because the spectrum was similar to that at Cilacap (Figure 3c). Minor data gaps (less than 3% of the data) were interpolated linearly. The power spectra showed a prominent intraseasonal signal of between 10 and 50 days in the data of each station, some of which exceeded the 90% confidence level of the red noise background. The data at Padang in Sumatra also displayed a significant peak of semiannual variability probably due to the semiannual Wyrtki jet, which is originally produced in the equatorial Indian Ocean. A significant annual peak was also observed at Benoa. There was also a notable spectral peak of around 14–15 days in each plot, which was the so-called fortnightly tidal variation produced from the two main semidiurnal tides [e.g., *Ffield and Gordon*, 1996]. Because our primary focus was the coastal upwelling signal, we did not focus on the 14–15 day tidal variability in this study. We also repeated the spectrum analysis using along-track SLA data at each of the nearest points from the tidal station. The results demonstrated that while the satellite-observed SLA had similar semiannual and annual spectral peaks, the intraseasonal spectral peaks, especially those on a time scale shorter than 30 days, were not captured in the SLA data (figure not shown).

Because active sea level fluctuations were expected to be related to variations in ocean temperature, we compared sea level variation at each tidal station with SST variation at each nearest neighboring grid point of the gridded TMI SST. As a result, the local SST signal associated with sea level variations was obtained

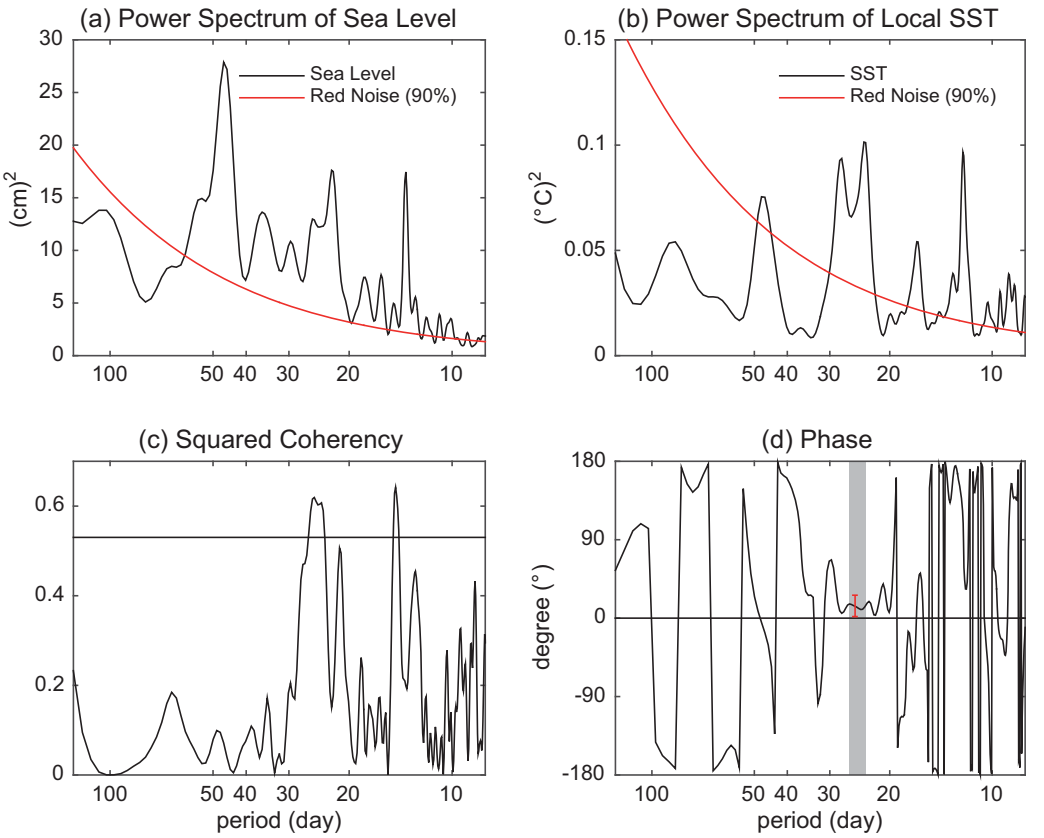

Figure 4. Variance-preserving spectra of (a) the sea level along the southern coast of Java and (b) the local SST (109°E–111°E, 8.5°S–9.5°S). A Hanning filter was applied 10 times to smooth the spectra. The red lines are the same as in Figure 3. (c) Squared coherency between the sea level and the SST. The 90% confidence limits are shown by the horizontal line. (d) The phase between the sea level and the SST. The period around 23–26 days, where the squared coherency is significant, is shaded, and the 90% confidence limits on the phase are shown as a red error bar. A positive phase indicates that the SST leads the sea level.

only along the southern coast of Java. Therefore, we examined the sea level at Cilacap and Prigi with the local SST (Figure 4). To prepare a long sea level time series along the southern coast of Java with no missing values, we merged two time series at Cilacap and Prigi for the period 2007–2012. Where data were available for both stations, we simply averaged the two data sets, or simply used one data set when the other was missing. The power spectrum of the sea level (Figure 4a) was almost identical to that at Cilacap (Figure 3c), but Figure 4 shows the intraseasonal time scale. We then calculated the power spectrum of SST, and the squared coherency and phase between the SST and the sea level variations. The SST off the coast of Java (109°E–111°E, 8.5°S–9.5°S) also exhibited significant intraseasonal spectral peaks, with the most pronounced peak of 22–30 days (Figure 4b). A significant peak of squared coherency was found at 23–26 days (Figure 4c). The phase difference was small (11°–16°) for the period and corresponded to a lag of only 1 day, in which SST leads the sea level.

The power spectra, squared coherency, and phase for the sea level at the southern coast of Sumatra (Panjang) and local SST off the coast (103°E–105°E, 5.0°S–7.0°S) are shown in supporting information Figure S1. Although the local SST exhibited some intraseasonal spectral peaks such as at periods around 20 day and 37–60 days, there was no significant peak of squared coherency around 20–30 days.

Iskandar et al. [2005] reported that both remote winds over the equatorial Indian Ocean and local alongshore winds produced intraseasonal variations of the sea level along the coasts of Sumatra and Java. To observe the wind forcing associated with the intraseasonal sea level variations in each spectral band, we calculated the power spectra of winds along the equator and along the coasts of Sumatra and Java (Figure 5a). We also examined the squared coherency and phase between the winds and the sea level along

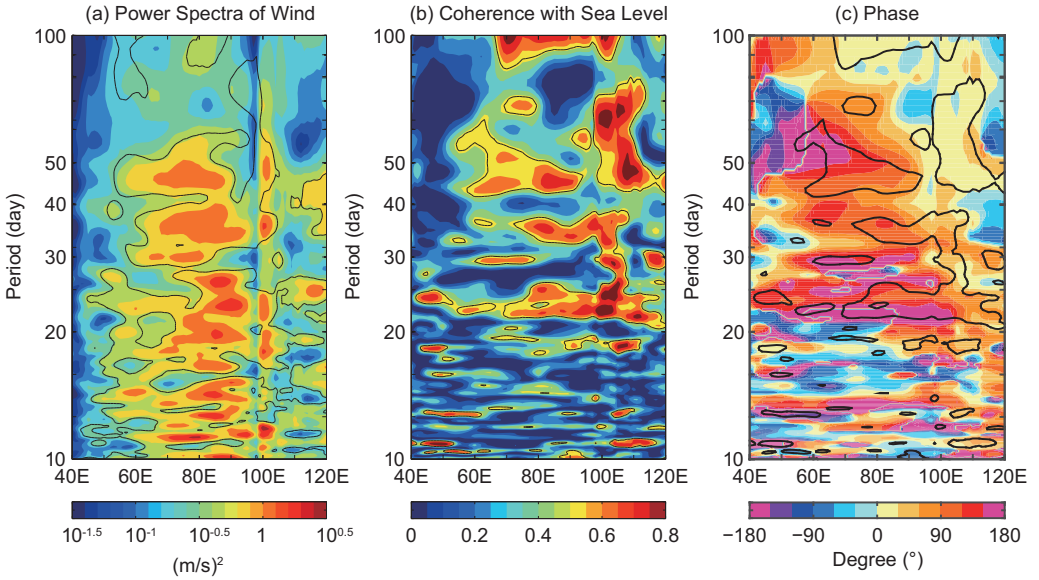

Figure 5. (a) Variance-preserving spectra of the wind time series along the equator (40°E–98°E) and along the coasts of Sumatra, Java, and Bali (98°E–120°E). A Hanning filter was applied 10 times to smooth the spectra. The contours denote the spectra with more than 90% confidence limits of the theoretical red noise background (the degree of freedom was estimated to be 16). (b) Squared coherency and (c) phase between the wind and the sea level along the southern coast of Java. The 90% confidence limits for the coherency are shown by the contours in both plots. A positive phase indicates that the winds lead the sea level.

the southern coast of Java (Figures 5b and 5c). A Hovmoller diagram of the wind spectra indicated significantly high energy levels over a broad range at periods of 10–60 days, which were observed across almost the entire equatorial Indian Ocean and along the coasts.

Significant peaks of squared coherency with the high spectra of the winds were observed at periods around 22–37 days along the coasts of Sumatra and Java, and at around 22–27, 33–37, and 43–50 days throughout the eastern Indian Ocean. Because the energy of the winds was low, we did not focus on spectral bands of more than 50 days. For periods of 20–50 days, which had significant values of squared coherency, phase differences ranged from 30° to 180°, indicating that winds lead sea level variations by around 4–10 days. There, the phase difference became larger in the westward direction, suggesting an atmospheric wind forcing that propagated from west to east. These results (Figures 4 and 5) indicate that the sea level along the southern coast of Java, the local SST there, and winds along the equator (40°E–98°E) and along the coasts (98°E–120°E) were correlated mainly at 20–30 day periods, with a peak at around 25 days at which sea level and SST are strongly correlated.

To examine seasonal differences in the linkage between the sea level and local SST variations, we conducted a seasonally stratified correlation analysis (Figure 6). In this analysis, we applied a Lanczos band-pass filter (20–30 day) and a time window of three consecutive months to the sea level time series during 2007–2012, and calculated the correlation with the local SST variations. The significant positive correlation expected in the cross spectrum (Figure 4) was only obtained during April–October, when southeasterly wind was dominant along the coast of Java and the sea level was relatively low. As discussed later, these signals were associated with intraseasonal atmospheric forcing that has broader spectral peaks than 20–30 days. Therefore, we also tested the result with a 20–50 day band-pass filter. The results were essentially same as shown in Figure 6b. These results indicate that the intraseasonal-scale lowering of sea level (or shoaling of the thermocline) during the summer monsoon was concurrent with the depression of local SST, probably through an oceanic one-dimensional vertical process. The SST was negatively correlated with the sea level during November–March (the boreal winter), implying that other thermodynamic processes, such as air-sea heat exchange, were more important in that season. The contributions of heat flux will be further diagnosed in the next section. We also tested the result, changing the cutoff period of the band-pass filter to 20–40 and 40–50 day. We confirmed that the modifications of the cutoff period did not produce a fundamental difference in the results.

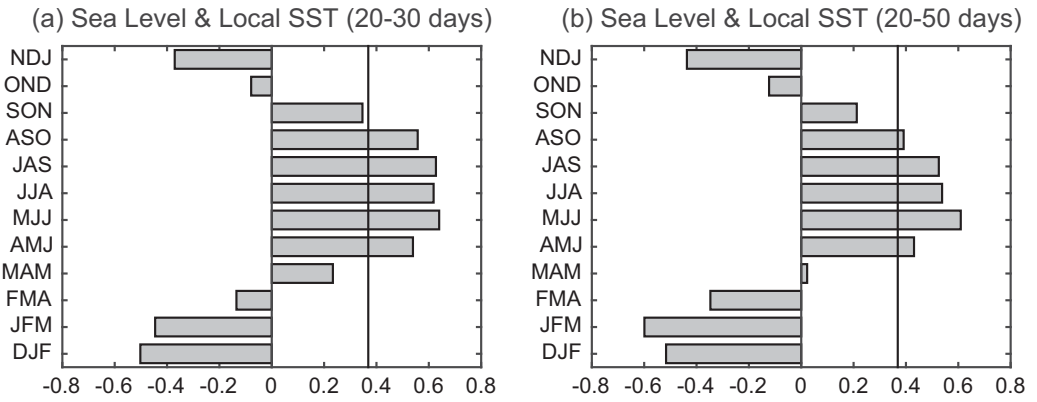

Figure 6. (a) Seasonally stratified correlation coefficients between the sea level and local SST variation at 8°S, 110°E. The data were filtered using a 61-point Lanczos filter to extract the 20–30 day signals. The dashed line indicates a statistically significant correlation at the 90% level, defined by the effective sampling number (20) in the analysis based on the autocorrelation coefficient. (b) As in Figure 6a, but for the data filtered using a 101-point Lanczos filter to extract the 20–50 day signals.

In summary, intraseasonal variations were apparent in the sea level, the local SST, and winds along the equator and the coasts of Sumatra and Java. The sea level and SST off the coast of Java were correlated with a time scale of 20–30 days only during the boreal summer monsoon. The sea level and winds were associated on an intraseasonal time scale of 20–50 days in which the winds led to sea level variations.

4. Coastal Upwelling Events and Local SST Variations

In this section, we focus on significant sea level variations on an intraseasonal time scale for each coastal upwelling event. We first extracted significant sea level drop (SLD) events from the long-term in situ data shown in Figure 2. As mentioned above, intraseasonal sea level and local SST variations were correlated only along the southern coast of Java. Therefore, we focused on sea level time series for the southern coast of Java. We then identified local and large-scale atmospheric and oceanic variations related to the sea level signals.

4.1. Intraseasonal Coastal Upwelling Signals in Long-Term Data

Coastal upwelling signals are closely associated with a lowering of the sea level because the upwelling, i.e., subsurface vertical velocity, is concurrent with thermocline shoaling [*Charney*, 1955; *Yoshida*, 1955; *Gill and Clarke*, 1974]. Using the simple method described below, we extracted significant SLD events as a proxy for coastal upwelling events. Using a sea level (hereafter "h") time series for the southern coast of Java, we defined a SLD event as a statistically significant lowering of h in 10 days ($\Delta h/\Delta t$). Here we preferred temporal change ($\Delta h/\Delta t$) to h because this procedure could remove the unfavorable effects of a datum shift. We used a difference interval of 10 days for a practical reason: we also conducted an analysis using an along-track SLA that had a 10 day repeat cycle. We set thresholds based on the standard deviation (σ) of $\Delta h/\Delta t$, and tested both 1.5σ and 2.0σ as a threshold to select the events. We examined SLD events along the southern coast of Java (Cilacap and Prigi) when in situ data for at least 1 month were available. To extend the period, we also analyzed the data at Bali and added the results to this analysis. As a result, 208 months for the 29 years (1984–2012) were examined. The standard deviation of $\Delta h/\Delta t$ (cm per 10 days) was 13.04 at Cilacap, 11.99 at Prigi, and 9.98 at Benoa. The SLD events (defined by a threshold of 2.0σ) are indicated in Figure 2.

The seasonal frequency of the significant SLD events observed in the 208 months is shown as a monthly histogram in Figure 7. Although there were some data gaps, the number of each monthly observation did not significantly vary (16–18). We also calculated the monthly occurrence ratio of SLD events and obtained same results (not shown). There were frequent signals in December–March and May–June, with a minor dip in April. A peak in the number of SLD events (Figure 7) in May–June was likely to be a manifestation of intraseasonal coastal upwelling under a southeasterly monsoonal wind. In June, intraseasonal-scale SLD events were most frequently observed. During the recession of the summer monsoon and subsequent transition period (September–October), signals were rarely observed probably because there were no intraseasonal

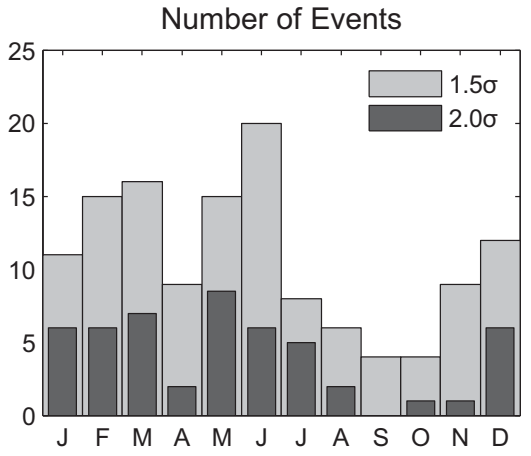

Figure 7. Monthly histogram showing the number of observed sea level drop (SLD) events observed along the southern coast of Java. The light-colored (dark-colored) bar indicates the statistics of the SLD events sampled on the basis of 1.5 (2.0) standard deviations. (The details are given in section 4.1.)

disturbances or southeasterly monsoonal winds. We also conducted the same analysis using along-track SLA and found that intraseasonal-scale SLD events were less well captured from satellite observations, as would be expected from Figure 2.

4.2. Coastal Upwelling and Local SST

Following the histogram (Figure 7) and the results presented in section 3, we further focused on the intraseasonal-scale SLD events that occurred during April–August. We prepared the same time series used in the section 3 (merged time series based on Cilacap and Prigi), and analyzed the data for the southern coast of Java. We focused on the period 2007–2012, during which we obtained relatively reliable in situ sea level observations and a high-resolution SST data set. Because there were fewer missing values for this period, we applied a Lanczos band-pass filter and extracted 20–50 day signals. The amplitude (the variance ratio to total variance) of the intraseasonal variations was 14.0 cm (5.4%) for sea level and 1.1°C (3.6%) for SST. Then we observed each intraseasonal variation and performed composite analyses, using the significant negative peaks in filtered sea level as the reference of day zero.

We used a threshold of 1.5σ of filtered sea level data to define 10 significant SLD events (Figure 8a). Note that in section 4.1, we simply used $\Delta h/\Delta t$ to define SLD events without applying a band-pass filter because there were a number of data gaps before 2006 that prevented applying the filter. In this subsection, to focus on the intraseasonal signals in sea level variation, we applied the 20–50 day band-pass filter for the period 2007–2012. As a result, several SLD events defined from $\Delta h/\Delta t$ (section 4.1) were smoothed out because these SLD events were probably related to the variation with shorter time scales less than 20 days. Note also that the changes in the definition and the minor modification of the cutoff period of the band-pass filtering did not produce a fundamental difference in the results.

Significant SLD events were accompanied by southeasterly alongshore wind anomalies a few days earlier and by concurrent cold SST anomalies (Figure 8). Although the amplitude of the winds varied between events, on average, the southeasterly winds along the coasts of Java peaked 6 days before the SLD peak. The composite peak (−1.86 m/s) was about 27% of the maximum of the climatological southeasterly wind. The wind signals from day −9 to day −3 before the peak were statistically significant at the 90% level (Figure 8d). The variance of the SST signals was large and the timing of the negative peaks of the SST anomalies varied between events. This implies that processes other than an oceanic one-dimensional process, such as air-sea heat exchange and horizontal heat advection, also controlled the intraseasonal SST variations. Nevertheless, the cold SST anomalies were statistically significant on days +1 and +2, suggesting that coastal upwelling had an impact on local SST.

Atmospheric and oceanic signals associated with the SLD events were also observed in the large-scale wind, satellite-observed SLA (MSLA product), and SST (Figure 9). A Hovmoller diagram indicated that southeasterly wind anomalies were significant along the coasts of Java and Sumatra (100°E–110°E) (Figure 9a). The signals could be tracked in the central equatorial Indian Ocean (70°E–85°E) up to day −15, when they were also statistically significant. There were also significant signals for the SLA anomalies that propagated west to east mainly along the coasts of Sumatra, Java, and Bali (Figure 9b). Although there were large easterly winds in the central equatorial Indian Ocean, the amplitude of the SLA was larger east of 90°E. The amplitude of the satellite-based data was up to 5 cm along the southern coast of Java, and was about half of that from in situ sea level observations. The west-to-east propagation of the atmospheric signal indicates that the Madden-Julian Oscillation [*Madden and Julian*, 1972] or summertime northward-propagating

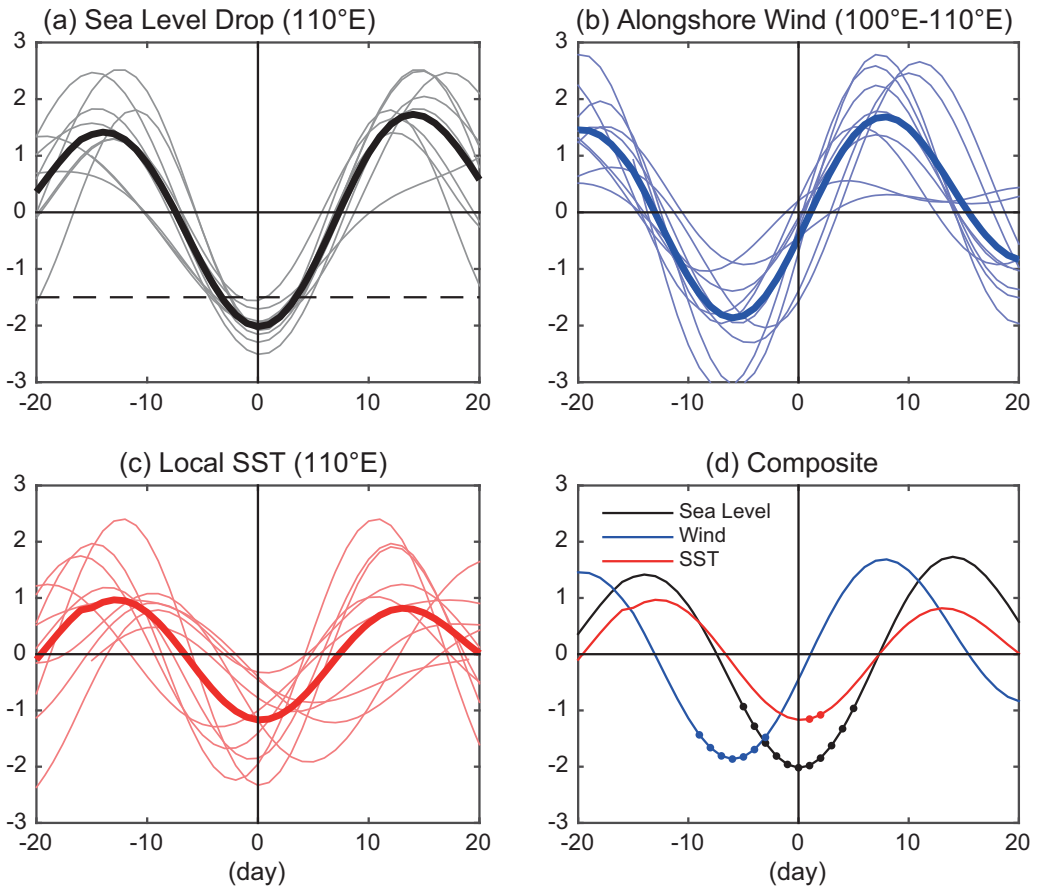

Figure 8. (a) Sea level anomalies for 10 observed sea level drop (SLD) events south of Java (110°E). The events observed in April–October of 2007–2012 were selected according to the criteria of the amplitude of the sea level drop being greater than a 1.5 standard deviation ($h < 1.5\sigma$). The thick line represents the composite of the events. (b) As in Figure 8a, but for the alongshore wind anomalies averaged for 100°E–110°E, based on the SLD events. (c) As in Figure 8b, but for the SST anomalies south of Java (110°E). (d) Composite time series of the data in Figures 8a–8c. The original time series are standardized so that the mean and one standard deviation were set to 0 and 1, respectively. The values with dots are statistically significant at the 90% level.

intraseasonal oscillations [*Lawrence and Webster*, 2002] probably produced the easterly and southeasterly wind anomalies.

Significant cold SST anomalies associated with the SLD events were observed only at a narrow range off the coast of Java (Figure 9c). The cold anomalies were confined around the peak of the SLD events from day −3 to day +3. Based on hydrostatic approximation, coastal upwelling, or subsurface upward vertical velocity, is concurrent with thermocline shoaling [*Charney*, 1955; *Yoshida*, 1955]. In other words, coastal upwelling is in phase with $\Delta h/\Delta t$. Considering the ocean heat balance, coastal upwelling could result in the SST cooling concurrent with the SLD. It should be also noted that the phase of the SST signals along the coasts (105°E–120°E) was different from that in the equatorial Indian Ocean (70°E–100°E). The SST variation in the equatorial Indian Ocean might be from air-sea flux variations associated with atmospheric intraseasonal variation, which will be discussed in the next section.

To examine the thermodynamic balance off the coast of Java, we analyzed local net surface heat flux (109°E–111°E, 9°S–8°S) around the peak of the SLD events. We applied the same band-pass (20–50 day) filter and observed composite time series of air-sea fluxes (Figure 10). To assess the impact on the local SST variation, contribution of the air-sea heat flux to the rate of change of the mixed layer temperature was estimated to be $(Q_0 - Q_{pen})/\rho C_p H$, where Q_0 is the net heat flux across the air-sea interface, Q_{pen} represents shortwave radiation which penetrates below the mixed layer, ρ is seawater density, C_p is heat capacity, and H is the mixed layer depth (MLD). We estimated Q_0 using TropFlux data sets and Q_{pen} was estimated using the equation for Type IA water proposed by *Paulson and Simpson* [1977]. ρ and C_p were set as constant

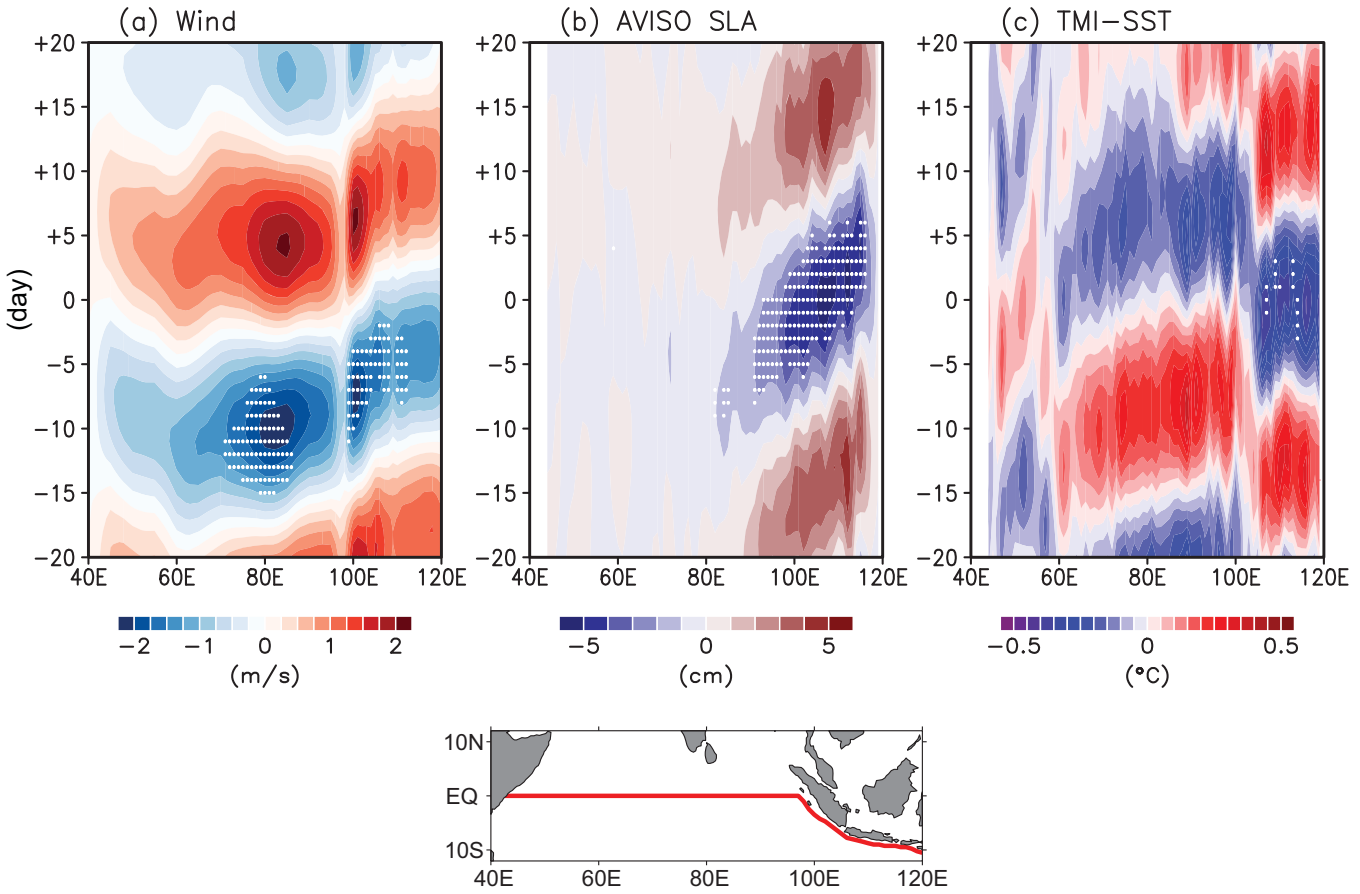

Figure 9. Longitude-time diagrams of band-pass filtered (a) NCEP wind, (b) AVISO Merged SLA, and (c) TMI SST along the equator (40°E–98°E) and along the coasts of Sumatra, Java, and Bali (98°E–120°E). The section is indicated in the bottom plot by the red line. Composite anomalies based on the peak (0 day) of sea level drop (SLD) events, as in Figure 8. Positive winds in Figure 9a indicate westerly (north-westerly) wind along the equator (coasts). The values with the white dots are statistically significant at the 90% level.

values of 1030 kg m^{-1} and 3930 J (kg °C)$^{-1}$, respectively. A climatological MLD based on Argo floats [*de Boyer Montégut et al.*, 2004] shows that the MLD near the southern coast of Java is 20–40 m. In reality, the MLD at the coastal area is unknown because of lack of observational data. In this analysis, we set a constant MLD of 10 ± 5 m as in *Shinoda and Hendon* [1998]. Note that a deeper MLD estimate could reduce the impact of heat flux on the mixed layer temperature considerably.

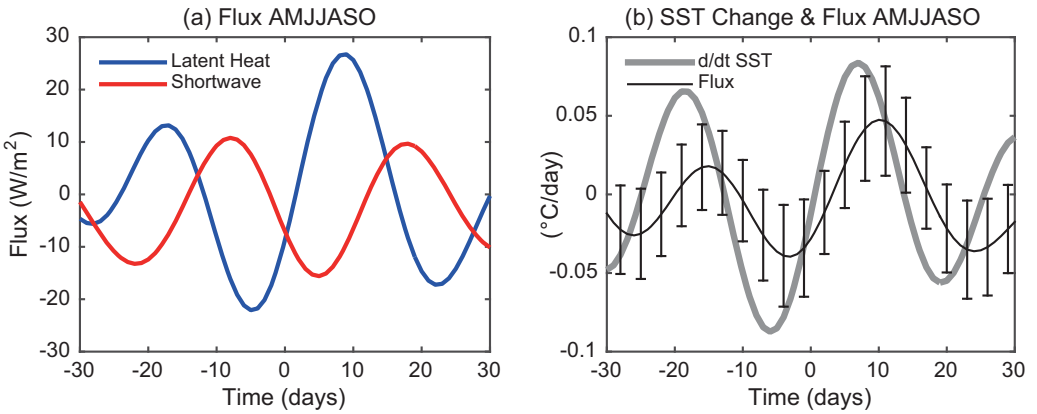

Figure 10. As in Figure 8d but for (a) composite time series of latent heat flux (blue) and shortwave radiation (red) and (b) contribution of net surface heat flux to the mixed layer (black) and temporal change of the SST. Positive heat flux indicates heat gain to the ocean. The vertical bars indicate the errors in the estimate of contribution of flux.

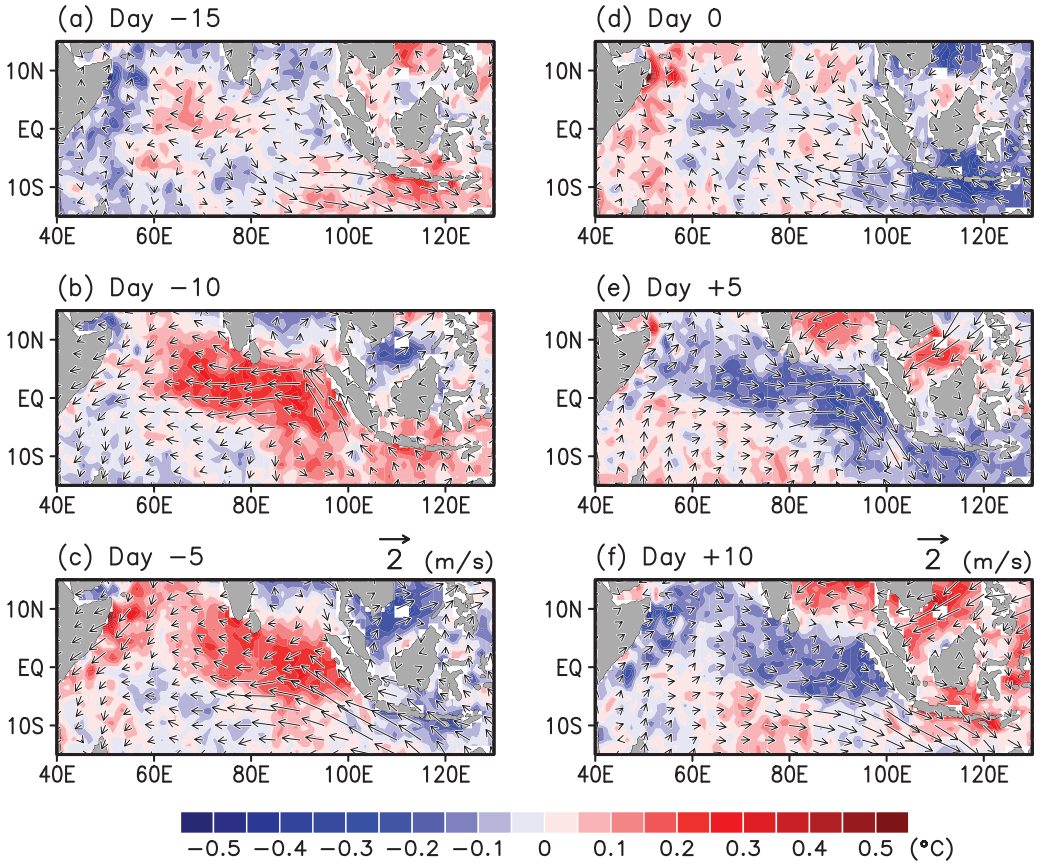

Figure 11. Composite maps of band-pass filtered SST anomalies (color shading) and surface wind anomalies (vector). The time shown in the title of each plot is relative to the peak of the SLD events.

The changes in the latent heat flux and shortwave radiation were the primary components of the net heat flux variation. Before the peak of SLD, enhanced latent heat flux due to strengthened southeasterly wind (from day −11 to day +1) and enhanced shortwave radiation (from day −13 to day −3) were counterbalanced (Figure 10a) and the SST cooling (from day −12 to day 0) could not be fully explained by the air-sea flux (Figure 10b). This implies that other process, such as coastal upwelling, may play a role in the SST cooling concurrent with SLD.

A horizontal map showed the cold SST anomalies that developed with southeasterly winds off the southern coasts of Java from day −10 day to day 0 (Figure 11). Easterly wind anomalies first appeared in the central equatorial Indian Ocean (day −15), and later covered the entire equatorial Indian Ocean with southeasterly wind anomalies along the coasts of Sumatra and Java (day −10). Cold SST anomalies first appeared off the southern coasts of Java and the Lesser Sunda Islands, with the southeasterly wind anomalies peaking around day −5. In this phase, positive SST anomalies located in the eastern equatorial Indian Ocean and a northwest-to-southeast gradient of SST anomalies were observed along the coastal area. As we discuss later, this anomalous SST gradient could enhance the seasonal SST gradient during the boreal summer. Cold SST anomalies developed and spread off the southern coasts (day 0), with anomalous cold SSTs also found in the Java Sea and Flores Sea. Cold SST anomalies spread over the central to southeastern tropical Indian Ocean on day +5, while wind anomalies had already turned to westerly (northwesterly) over the equatorial Indian Ocean (along the coasts of Sumatra and Java). After a few days, the cold SST anomalies ceased off the coasts of Java (day +10).

These results indicate that the intraseasonal-scale signals of the lowering of sea level along the southern coast of Java were associated with basin-scale anomalous atmospheric circulation during the boreal summer monsoon. Anomalous southeasterly wind along the coast of Java, the resultant offshore Ekman transport, and possible coastal upwelling were consistent with SST cooling, concurrent with the sea level

lowering signal. Although the signals were not statistically significant at the 90% level, cold SST anomalies also appeared in the central-eastern equatorial Indian Ocean, with a different phase from those in the coastal area. This suggests that a different process, such as the air-sea heat flux, played a more important role in the open-ocean SST variations. The implications of these observations for regional air-sea interaction are discussed in the next section.

5. Discussion

The long-term sea level observation data from Indonesian tidal stations provide an excellent opportunity to study the intraseasonal sea level variations associated with coastal upwelling signals along the southern coast of Java. Previous studies used satellite-observed SST and sea level data to show seasonal to interannual signals of the coastal upwelling. However, coastal upwelling phenomena have a time scale of a few days or weeks as suggested by previous studies [e.g., *Charney*, 1955; *Yoshida*, 1955]. Therefore, understanding the energetic upwelling variations on these time scales requires temporally high-resolution observations. Following *Iskandar et al*. [2005], who clarified sea level variations in terms of their dynamics, we also examined the relationship between the sea level and local SST by using a recent high-resolution satellite SST data set. The coastal area was located in the Indian Ocean warm pool so that the implications of the coastal upwelling signals associated with local SST cooling and hence possible air-sea interactions are discussed here.

Focusing on SLD events as a proxy for coastal upwelling, this study extracted the signal of intraseasonal SST cooling concurrent with coastal upwelling. During the boreal summer, intraseasonal SLD events are likely related to coastal upwelling under a southeasterly monsoonal wind. Upwelling Kelvin waves that propagate along the coasts of Sumatra and Java can also explain the observed SLD events. *Drushka et al*. [2010] extracted upwelling Kelvin waves forced by intraseasonal easterly wind anomalies during both boreal summer and winter. In our definition of SLD events, the signal of upwelling Kelvin waves could also produce significant signals in sea level variation. To distinguish a signal of coastal upwelling and that from upwelling Kelvin waves, however, an extended analysis using several tidal station data along the coasts of Sumatra and Java would be needed in the future.

To discuss the significance of the sea level variation in thermodynamic balance, we conducted linear regression analyses using ocean observation data in the eastern Indian Ocean. Based on dynamical analogy between coastal upwelling and equatorial upwelling [e.g., *Gill and Clarke*, 1974], we examined ocean profile data on the equator from a moored buoy of the Research Moored Array for African-Asian-Australian Monsoon Analysis and Prediction (RAMA) [*McPhaden et al*., 2009] at 0°, 90°E. Using the buoy data for the period of 9 November 2004 to 7 April 2013, we calculated dynamic height and depth of the 20°C isotherm as measures of sea level and main thermocline, respectively. The results indicated that a significant dynamic height decrease with the amplitude of 10 cm explained main thermocline uplift more than 22 m. The thermocline variation is in the order of that at the onset phase of positive IOD, as observed in *Horii et al*. [2008]. In this study, we also examined the statistical relationship between sea level and local SST along the coast of Java during the summer monsoon (May–August). We found that the SLD event of 10 cm explained intraseasonal-scale SST decrease of more than 0.38°C. Given the high background SST condition close to the deep convection threshold, SST decrease due to coastal upwelling could have an effect on suppressing convection.

The intraseasonal SST signal observed during April–October was actually embedded into seasonal SST evolution during the summer monsoon. Figure 12 shows composite maps based on the SLD events as in Figure 11, but using raw SST and surface wind instead. It shows that there was a persistent summer monsoonal circulation, in which southeasterly winds were predominant along the coasts of Sumatra and Java. From Figure 11, it can be seen that the southeasterly monsoonal wind had a maximum from day −10 to day 0 and an anomalous cold SST developed off the southern coasts of Java and the Lesser Sunda Islands from day −10 to day 0. The decrease of SST off the coast of Java (110°E–120°E, 12°S–8°S) was rapid, with a decline from 29.5°C (day −10) to 28.3°C (day 0). The anomalous cold SST also formed a large SST gradient along the coast of Java, which was similar to the climatological SST (Figure 1) in terms of its pattern.

Can the anomalous SST produce active air-sea interaction in this area? Assuming a Gill-type atmospheric response [*Matsuno*, 1966; *Gill*, 1980] for the off-equatorial cold SST, a descending atmospheric Rossby wave

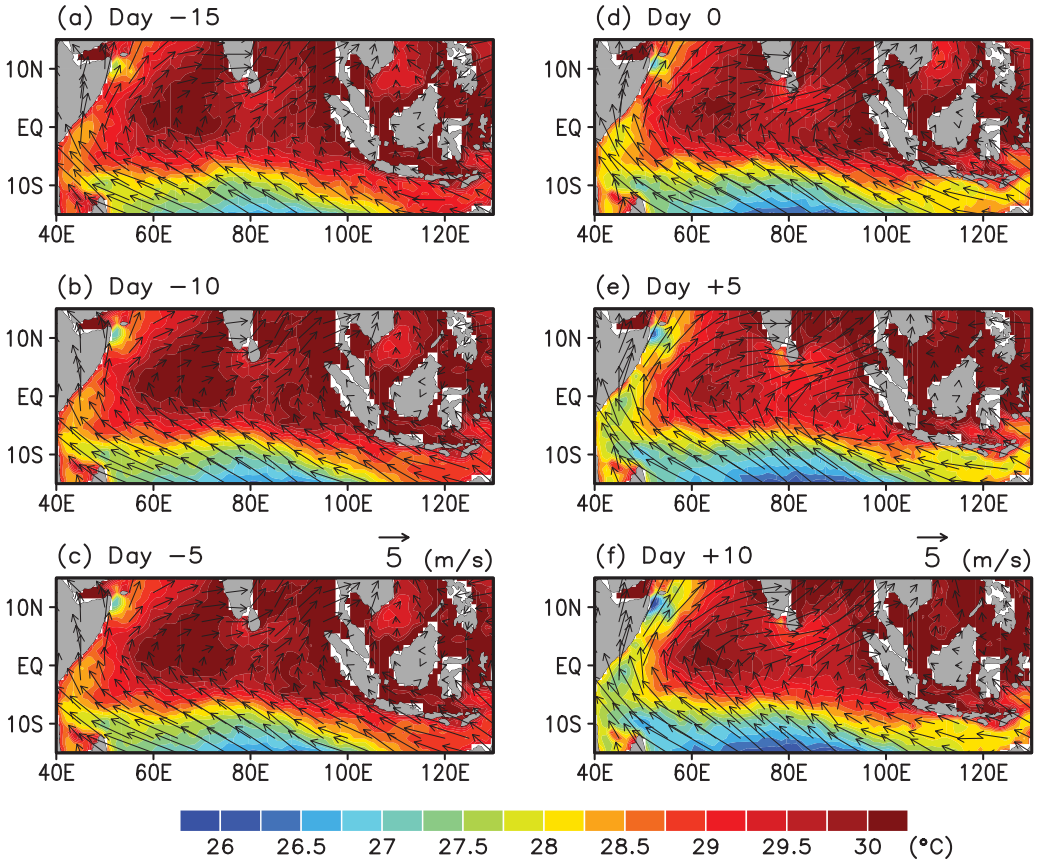

Figure 12. As in Figure 11, but composite maps of raw SST (color shading) and the surface wind (vector).

response produces an anomalous anticyclonic circulation to the west. As suggested by *Li et al*. [2003], the anticyclonic circulation off the coasts of Sumatra and Java is favorable to the enhancement of southeasterly wind, which was originally responsible for the coastal upwelling. They also suggested that the anomalous circulation could cool the SST through an enhanced latent heat flux and vertical mixing. The atmospheric reanalysis data set provided little evidence (not shown), probably because the reanalysis data were forced by optimum interpolation (OI) SST, and were not suitable for reproducing a regional-scale phenomenon. Further observations and analyses, focusing on the area off the coast of Java, are needed to improve the estimation of the atmospheric response to the local SST, and hence the local air-sea interaction in the southeastern tropical Indian Ocean.

While we focused on the SST around the coastal area, basin-scale SST in the equatorial Indian Ocean also fluctuated with the intraseasonal sea level variation (Figures 9 and 11). This suggests that large-scale atmospheric intraseasonal oscillations during the summer monsoon [*Lawrence and Webster*, 2002] produced such SST anomalies, and that the primary process to control the SST variations differed between the coastal area and the open ocean. In general, the intraseasonal oscillation produces an anomalous SST through first anomalous shortwave radiation and then the latent heat flux [e.g., *Shinoda et al*., 1998]. The variations of shortwave radiation lead those of the latent heat flux in the tropical Indian Ocean [*Shinoda and Hendon*, 1998; *Schiller and Godfrey*, 2003]. We checked the variations of NOAA outgoing longwave radiation (OLR) data and TropFlux shortwave radiation during the SLD events and found that a convective peak was located in the central-eastern tropical Indian Ocean from day −3 to +2 (not shown), with respective to the negative peaks of the sea level (Figure 8). Shortwave radiation should be suppressed during this phase, and probably leads to cold SST anomalies by around days +3 to +8 (Figures 9 and 10). Considering the wind system along the coasts of Sumatra, Java, and Bali (98°E–120°E) is characterized by the same southeasterly monsoonal wind in this season, the spatial change in the SST variation along the coasts found around 105°E may indicate specific thermodynamic balance off the coasts of Java.

Along the coast of Java, an enhanced latent heat flux could also produce cold SST anomalies [*Li et al*., 2003; *Tokinaga and Tanimoto*, 2004]. Superimposed on the climatological southeasterly wind, the wind speed off the coast of Java was at a maximum around day −5, when a decreasing SST was observed in the coastal area. The resulting enhancement of evaporative cooling during this phase could also explain the spread of anomalously cold SST into the southeastern tropical Indian Ocean from day −5 to day 0 (Figure 11d). Using an Oceanic General Circulation Model (OGCM) for the Earth Simulator (OFES), *Du et al*. [2005] examined seasonal mixed layer heat budgets in the southeastern tropical Indian Ocean, including the coastal area that was the focus of this study. Although they focused on a seasonal time scale, their results indicated that both the surface heat flux and coastal upwelling contributed to cooling during June–September. They also suggested that the effect from coastal upwelling was twice as large as that from the surface heat flux, and was partly compensated by warm-water advection through the Indonesian throughflow. However, their conclusion was based on numerical modeling and applied to seasonal-scale mixed layer temperature variation in the southeastern tropical Indian Ocean. Further studies are needed to evaluate if their conclusions from numerical modeling are consistent with regard to intraseasonal ocean temperature variations.

While this study focused on the sea level variation and local SST off the coast of Java during the boreal summer, we note that we have also obtained completely different results for the relationship between sea level and local SST variations during boreal winter (November–March). As seen in the significant negative correlation during winter (Figure 6), a SLD event was accompanied by warm SST anomalies in this season (supporting information Figure S2). This can be caused by atmospheric forcing associated with MJO during boreal winter: a convective (dry) phase of MJO in the eastern tropical Indian Ocean is characterized by westerly (easterly) winds with decreased (increased) surface heat flux from atmosphere to ocean decreased because of the suppressed (enhanced) short wave radiation and enhanced (reduced) latent heat flux [e.g., *Shinoda et al*., 1998]. The SLD events at the southern coast of Java corresponded to dry phase with anomalous easterly southeasterly winds propagated from the equatorial central Indian Ocean (supporting information Figure S2). The contribution of heat flux to the mixed layer temperature was in phase with the temporal change in SST variation (supporting information Figure S3). Concurrent anomalous easterly winds along the coasts of Sumatra and Java [*Wheeler and Hendon*, 2004] could drive upwelling Kelvin waves. As a result, it is likely that warm SST anomalies were observed with SLD.

Finally it is of interest to know if the coastal upwelling and resulting SST cooling signal during the boreal summer is related to the occurrence of a seasonal basin-scale atmosphere-ocean coupling mode, i.e., the IOD [*Saji et al*., 1999; *Webster et al*., 1999]. Intraseasonal-scale disturbances can have an impact on the IOD [e.g., *Rao and Yamagata*, 2004]. Although we found a slight tendency for more SLD events before the onset of a positive IOD, the short period of reliable in situ data (2007–2012) prevented us from obtaining significant statics. In addition, only minor and moderate IOD events occurred during 2007–2012 [*Du et al*., 2013; *Horii et al*., 2013], and in situ sea level data for the southern coast of Java were missing during significant IOD events such as those in 1994, 1997, and 2006. We are currently attempting to reconstruct the coastal upwelling signal using neighboring sea level data and will present the statistical analysis of the coastal upwelling signal and the occurrence of IOD in future reports.

6. Summary and Conclusions

We have identified intraseasonal-scale coastal upwelling signals along the southern coast of Java from in situ sea level data. The sea level variations had a significant coherence with local SST (remote and local winds) with an intraseasonal time scale of 20–30 days (20–50 days). We focused on intraseasonal-scale SLD events as a proxy for coastal upwelling signals. Anomalous southeasterly wind, which then caused offshore Ekman transport and hence coastal upwelling, was found along the coasts of Sumatra and Java before the SLD event. A significant basin-scale signal of winds was also found in the central Indian Ocean up to 15 days before the SLD event, suggesting that atmospheric intraseasonal oscillations [*Lawrence and Webster*, 2002] was also effective for producing the southeasterly wind anomalies. The SST variations concurrent with the SLD events were significant off the southern coast of Java. Ocean entrainment cooling due to coastal upwelling or enhanced evaporative cooling explained the SST variation, unlike in the open-ocean SST which was probably controlled by the surface heat flux.

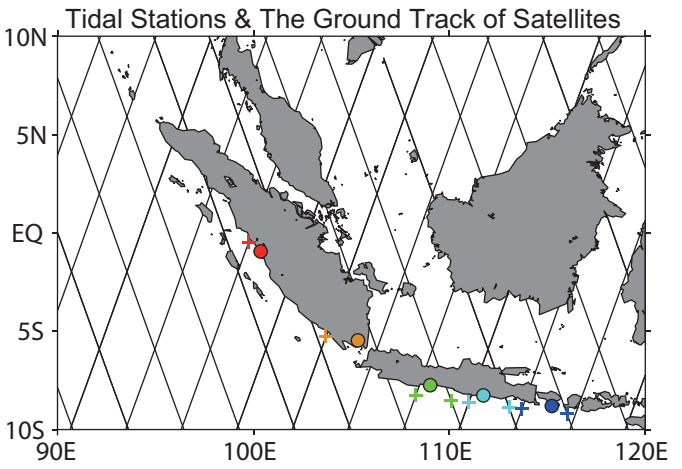

Figure A1. Locations of tidal stations and the ground track of AVISO satellites. Along-track SLA data shown by crosses were used for data comparison.

The intraseasonal-scale coastal upwelling signals and the statistical relationship with the local SST cooling enable a better understanding of the coastal upwelling system in the eastern boundary region of the Indian Ocean. Because it is unclear how ocean temperature fluctuates with the upwelling signal, future observations around the coasts of Sumatra and Java are needed to clarify the thermodynamic balance. In addition, the anomalous SST gradient concurrent with the coastal upwelling signal can enhance the seasonal SST gradient during the boreal summer, suggesting a possible effect on local air-sea interactions. Intensive atmosphere and ocean observations are therefore required to not only better understand coastal upwelling itself, but also to determine whether the large SST gradient drives active air-sea interaction over the area.

Appendix A: Validation of the Sea Level Data

In this appendix, we evaluate the sea level data observed by the Indonesian tidal stations by comparing them with the along-track SLA provided by AVISO. Tidal data must contain topographic effects, such as the topographic tide and topographic wave, and the tidal data and satellite altimetry, which focuses mainly on

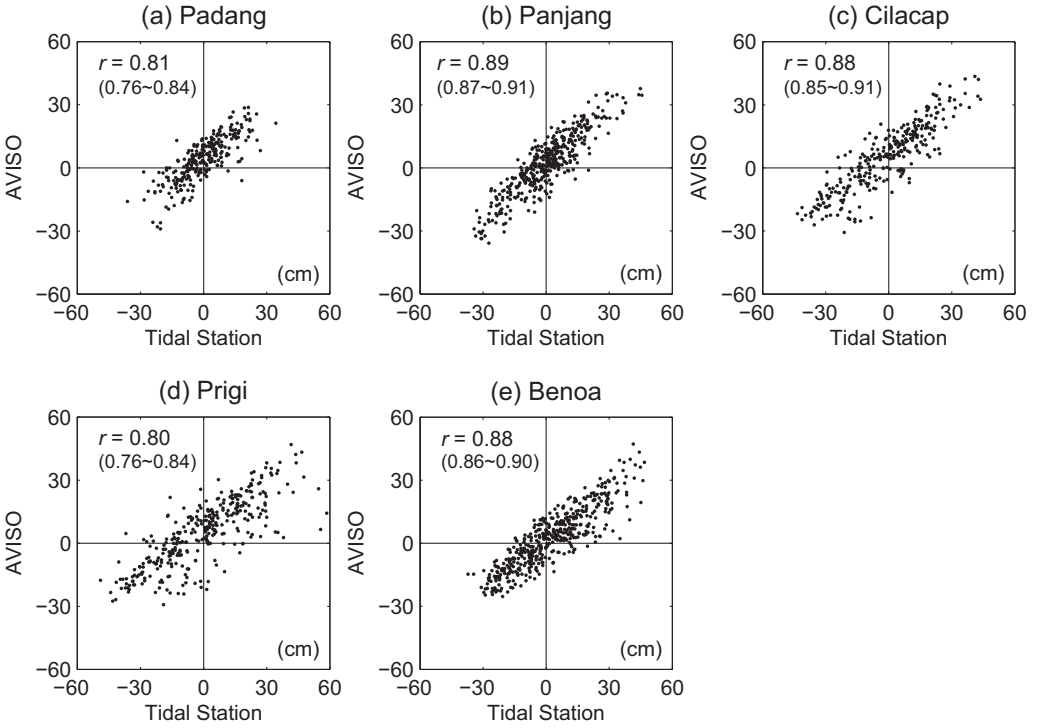

Figure A2. Comparison of sea level anomalies (cm) obtained from hourly tidal station data and those from the 10 day AVISO satellite data. (a) Padang, (b) Panjang, (c) Cilacap, (d) Prigi, and (e) Benoa. The correlation coefficient and confidence interval are given in the upper left-hand side of each plot. Each *p* value was less than 0.0001.

the open ocean, will not necessarily be in agreement. Nevertheless, we believe that this comparison of two independent data sets provides a guide for the credibility of the Indonesian tidal data.

To compare the sea level data at Padang and Panjang with satellite observations, we used along-track SLA data at each of the nearest open-ocean points from the tidal station (Figure A1). For other stations (Cilacap, Prigi, and Benoa), we used an ascending and descending track of satellite passes through the west and east side, respectively. Therefore, we used two satellite observation points to locate the nearest western and eastern points from each tidal station, and averaged them in terms of the value and time. In general, the time difference between the ascending and descending data was 12 h. The processed along-track SLA data provided a discrete time series, with an interval of almost 10 days.

In situ sea level data were plotted with satellite-observed SLA data for the period of 14 October 1992 to 31 December 2012, in cases where both observations were available (Figure A2). Significant correlations of more than 0.8 were obtained. The correlations at Padang and Prigi were relatively low. The reason for this may be the seafloor topography around Padang, in which a shallow bathymetry of less than 1000 km extended offshore to the Sunda Islands. In addition, the effects of a datum shift remained in the data from Prigi, which may be the cause of the large differences in the data. Overall, the tidal station data agreed well with satellite observations and ensure the validity of the conclusions of this study.

Acknowledgments

We thank UHSLC (http://uhslc.soest.hawaii.edu) for providing quality-controlled sea level data from tide gauges. We also thank the following data providers. The altimeter products were produced by Ssalto/Duacs and distributed by Aviso, with support from CNES; NOAA OISST data and NCEP reanalysis data were provided by the NOAA/OAR/ESRL PSD, Boulder, Colorado, USA, from their Web site (http://www.esrl.noaa.gov/psd/); TMI SST data were provided by Remote Sensing Systems (available online at http://www.remss.com). We thank two anonymous reviewers for valuable comments and suggestions. We also thank D. Yamanaka for helpful discussions. This study is financially supported by the Ministry of Education, Culture, Sports, Science and Technology, Japan, Grants-in-Aid for Scientific Research for Young Scientists (B), 25800270.

References

Akima, H. (1970), A new method of interpolation and smooth curve fitting based on local procedures, *J. Assoc. Comput. Mach.*, *17*, 589–602.

Bray, N. A., S. Hautala, J. C. Chong, and J. Pariwono (1996), Large-scale sea level, thermocline, and wind variations in the Indonesian Throughflow region, *J. Geophys. Res.*, *101*, 12,239–12,254.

Charney, J. G. (1955), The generation of oceanic currents by winds, *J. Mar. Res.*, *14*, 477–498.

Clark, N. E., L. Eber, R. M. Laurs, J. A. Renner, and J. F. T. Saur (1974), Heat exchange between ocean and atmosphere in the eastern North Pacific for 1961–1971, *NOAA Tech. Rep. NMRS SSRF-682*, pp. 108, NOAA, U. S. Dep. of Commer., Washington, D. C.

de Boyer Montégut, C., G. Madec, A. S. Fischer, A. Lazar, and D. Iudicone (2004), Mixed layer depth over the global ocean: An examination of profile data and a profile-based climatology, *J. Geophys. Res.*, *109*, C12003, doi:10.1029/2004JC002378.

Drushka, K., J. Sprintall, S. Gille, and I. Brodjonegoro (2010), Vertical structure of Kelvin waves in the Indonesian Throughflow, *J. Phys. Oceanogr.*, *40*(9), 1965–1987, doi:10.1175/2010JPO4380.1.

Du, Y., T. Qu, G. Meyers, Y. Masumoto, and H. Sasaki (2005), Seasonal heat budget in the mixed layer of the southeastern tropical Indian Ocean in a high resolution general circulation model, *J. Geophys. Res.*, *110*, C04012, doi:10.1029/2004JC002845.

Du, Y., W. Cai, and Y. Wu (2013), A new type of the Indian Ocean Dipole since the mid-1970s, *J. Clim.*, *28*, 959−972.

Ffield, A., and A. L. Gordon (1996), Tidal mixing signatures in the Indonesian Seas, *J. Phys. Oceanogr.*, *26*, 1924–1937.

Foreman, M. G. G. (1977), Manual for tidal heights analysis and prediction, *Pac. Mar. Sci. Rep. 77–10*, 58 pp., Inst. of Ocean Sci., Sidney, B. C.

Gill, A. E. (1980), Some simple solutions for heat-induced tropical circulation, *Q. J. R. Meteorol. Soc.*, *106*, 447–462.

Gill, A. E., and A. J. Clarke (1974), Wind-induced upwelling, coastal currents and sea-level changes, *Deep Sea Res. Oceanogr. Abstr.*, *21*, 325–345.

Halkides, D. J., and T. Lee (2009), Mechanisms controlling seasonal-to-interannual mixed layer temperature variability in the southeastern tropical Indian Ocean, *J. Geophys. Res.*, *114*, C02012, doi:10.1029/2008JC004949.

Hanawa, K., and H. Mitsudera (1985), On the data processing of daily mean values of oceanographic data: Note on the daily mean sea-level data [in Japanese], *Bull. Coastal Oceanogr.*, *23*, 79–87.

Horii, T., H. Hase, I. Ueki, and Y. Masumoto (2008), Oceanic precondition and evolution of the 2006 Indian Ocean dipole, *Geophys. Res. Lett.*, *35*, L03607, doi:10.1029/2007GL032464.

Horii, T., Y. Masumoto, I. Ueki, H. Hase, and K. Mizuno (2009), Mixed layer temperature balance in the eastern Indian Ocean during the 2006 Indian Ocean dipole, *J. Geophys. Res.*, *114*, C07011, doi:10.1029/2008JC005180.

Horii, T., I. Ueki, and K. Ando (2013), Contrasting development and decay processes of Indian Ocean Dipoles in the 2000s, *SOLA*, *9*, 183–186, doi:10.2151/sola.2013-041.

Iizuka, S., T. Matsuura, and T. Yamagata (2000), The Indian Ocean SST dipole simulated in a coupled general circulation model, *Geophys. Res. Lett.*, *27*, 3369–3372.

Iskandar, I., W. Mardiansyah, Y. Masumoto, and T. Yamagata (2005), Intraseasonal Kelvin waves along the southern coast of Sumatra and Java, *J. Geophys. Res.*, *110*, C04013, doi:10.1029/2004JC002508.

Iskandar, I., Y. Masumoto, K. Mizuno, H. Sasaki, A. K. Affandi, D. Setiabudidaya, and F. Syamsuddin (2014), Coherent intraseasonal oceanic variations in the eastern equatorial Indian Ocean and in the Lombok and Ombai Straits from observations and a high-resolution OGCM, *J. Geophys. Res. Oceans*, *119*, 615–630, doi:10.1002/2013JC009592.

Kalnay, E., et al. (1996), The NCEP/NCAR 40-year reanalysis project, *Bull. Am. Meteorol. Soc.*, *77*, 437–471.

Lawrence, D. M., and P. J. Webster (2002), The boreal summer intraseasonal oscillation: Relationship between northward and eastward movement of convection, *J. Atmos. Sci.*, *59*, 1593–1606.

Li, T., B. Wang, C.-P. Chang, and Y. Zhang (2003), A theory for the Indian Ocean dipole-zonal mode, *J. Atmos. Sci.*, *60*, 2119–2135.

Madden, R. A., and P. R. Julian (1972), Description of global scale circulation cell in the tropics with a 40-50 day period, *J. Atmos. Sci.*, *29*, 1109–1123.

Matsuno, T. (1966), Quasi-geostrophic motions in the equatorial area, *J. Meteorol. Soc. Jpn.*, *44*, 25–43.

McPhaden, M. J., G. Meyers, K. Ando, Y. Masumoto, V. S. N. Murty, M. Ravichandran, F. Syamsudin, J. Vialard, L. Yu, and W. Yu (2009), RAMA: The research moored array for African-Asian-Australian monsoon analysis and prediction, *Bull. Am. Meteorol. Soc.*, *90*(4), 459–480.

Murtugudde, R., J. P. McCreary, and A. J. Busalacchi (2000), Oceanic processes associated with anomalous events in the Indian Ocean with relevance to 1997–1998, *J. Geophys. Res.*, *105*, 3295–3306.

Ningsih, N. S., N. Rakhmaputeri, and A. B. Harto (2013), Upwelling variability along the southern coast of Bali and in Nusa Tenggara waters, *Ocean Sci. J.*, *48*(1), 49–57.
Paulson, C. A., and J. J. Simpson (1977), Irradiance measurements in the upper ocean, *J. Phys. Oceanogr.*, *7*, 952–956.
Pawlowicz, R., B. Beardsley, and S. Lentz (2002), Classical tidal harmonic analysis including error estimates in MATLAB using T_TIDE, *Comput. Geosci.*, *28*, 929–937.
Praveen Kumar, B., J. Vialard, M. Lengaigne, V. Murty, and M. J. McPhaden (2012), Tropflux: Air-sea fluxes for the global tropical oceans–description and evaluation, *Clim. Dyn.*, *38*, 1521–1543, doi:10.1007/s00382-012-1455-4.
Rao, S. A., and T. Yamagata (2004), Abrupt termination of Indian Ocean dipole events in response to intraseasonal disturbances, *Geophys. Res. Lett.*, *31*, L19306, doi:10.1029/2004GL020842.
Reynolds, R. W., N. A. Rayner, T. M. Smith, D. C. Stokes, and W. Wang (2002), An improved in situ and satellite SST analysis for climate, *J. Clim.*, *15*, 1609–1625.
Reynolds, R. W., T. M. Smith, C. Liu, D. B. Chelton, K. S. Casey, and M. G. Schlax (2007), Daily high-resolution-blended analyses for sea surface temperature, *J. Clim.*, *20*, 5473–5496.
Saji, N. H., B. H. Goswami, P. N. Vinayachandran, and T. Yamagata (1999), A dipole mode in the tropical Indian Ocean, *Nature*, *401*, 360–363.
Schiller, A., and J. S. Godfrey (2003), Indian Ocean intraseasonal variability in an ocean general circulation model, *J. Clim.*, *16*, 21–39.
Schott, F. A., S.-P. Xie, and J. P. McCreary Jr. (2009), Indian Ocean circulation and climate variability, *Rev. Geophys.*, *47*, RG1002, doi:10.1029/2007RG000245.
Shinoda, T., and H. H. Hendon (1998), Mixed layer modeling of intraseasonal variability in the tropical western Pacific and Indian Oceans, *J. Clim.*, *11*, 2668–2685.
Shinoda, T., H. H. Hendon, and J. Glick (1998), Intraseasonal variability of surface fluxes and sea surface temperature in the tropical western Pacific and Indian Oceans, *J. Clim.*, *11*, 1685–1702.
Sprintall, J., J. T. Potemra, S. L. Hautalac, N. A. Bray, and W. W. Pandoe (2003), Temperature and salinity variability in the exit passages of the Indonesian Throughflow, *Deep Sea Res., Part II*, *50*, 2183–2204.
Steinke, S., M. Prange, C. Feist, J. Groeneveld, and M. Mohtadi (2014), Upwelling variability off southern Indonesia over the past two millennia, *Geophys. Res. Lett.*, *41*, 7684–7693, doi:10.1002/2014GL061450.
Susanto, R. D., and J. Marra (2005), Effects of the 1997/98 El Niño on Chlorophyll a variability along the southern coasts of Java and Sumatra, *Oceanography*, *18*(4), 124–127, doi:10.5670/oceanog.2005.13.
Susanto, R. D., A. L. Gordon, and Q. N. Zheng (2001), Upwelling along the coasts of Java and Sumatra and its relation to ENSO, *Geophys. Res. Lett.*, *28*, 1599–1602.
Syamsudin, F., and A. Kaneko (2013), Ocean variability along the southern coast of Java and Lesser Sunda Islands, J. *Oceanogr.*, *69*(5), 557–570.
Tokinaga, H., and Y. Tanimoto (2004), Seasonal transition of SST anomalies in the tropical Indian Ocean during El Niño and Indian Ocean Dipole years, *J. Meteorol. Soc. Jpn.*, *82*, 1007–1018.
Vinayachandran, P. N., S. Iizuka, and T. Yamagata (2002), Indian Ocean dipole mode events in an ocean general circulation model, *Deep Sea Res., Part II*, *49*, 1573–1596.
Webster, P. J., A. M. Moore, J. P. Loschnigg, and R. R. Leben (1999), Coupled ocean-atmosphere dynamics in the Indian Ocean during 1997-98, *Nature*, *401*, 356–360.
Wentz, F. J. (1997), A well-calibrated ocean algorithm for special sensor microwave/imager, *J. Geophys. Res.*, *102*, 8703–8718.
Wheeler, M. C., and H. H. Hendon (2004), An all-season real-time multivariate MJO index: Development of an index for monitoring and prediction, *Mon. Weather Rev.*, *132*, 1917–1932.
Wyrtki, K. (1962), The upwelling in the region between Java and Australia during the south east monsoon, Aust. *J. Mar. Freshwater Res.*, *17*, 217–225.
Yamagata, T., K. Mizuno, and Y. Masumoto (1996), Seasonal variations in the equatorial Indian Ocean and their impact on the Lombok throughflow, *J. Geophys. Res.*, *101*, 12,465–12,473.
Yoshida, K. (1955), Coastal upwelling off the California coast, *Rec. Oceanogr. Works Jpn.*, *15*, 1–13.
Zhang, Y. C., W. B. Rossow, A. A. Lacis, V. Oinas, and M. I. Mishchenko (2004), Calculation of radiative fluxes from the surface to top of atmosphere based on ISCCP and other global data sets: Refinements of the radiative transfer model and the input data, *J. Geophys. Res.*, *109*, D19105, doi:10.1029/2003JD004457.